

Trapped particle evolution driven by residual gas collisions

Avinash Deshmukh¹, Riley A. Stewart¹, Pinrui Shen¹, James L. Booth², and Kirk W. Madison^{1,*}

¹*Department of Physics & Astronomy, University of British Columbia,
6224 Agricultural Road, Vancouver, B.C., V6T 1Z1, Canada*

²*Physics Department, British Columbia Institute of Technology,
3700 Willingdon Avenue, Burnaby, B.C. V5G 3H2, Canada.*

**Corresponding author: madison@phas.ubc.ca*

(Dated: October 10, 2023)

We present a comprehensive mathematical model and experimental measurements for the evolution of a trapped particle ensemble driven by collisions with a room-temperature background vapor. The model accommodates any trap geometry, confining potential, initial trapped distribution, and other experimental details; it only depends on the probability distribution function $P_t(E)$ for the collision-induced energy transfer to the trapped ensemble. We describe how to find $P_t(E)$ using quantum scattering calculations and how it can be approximated using quantum diffractive universality [1]. We then compare our model to experimental measurements of a ⁸⁷Rb ensemble energy evolution exposed to a room temperature background gas of Ar by means of a single parameter fit for the total collision rate Γ . We extracted a collision rate of $\Gamma = 0.646(1) \text{ s}^{-1}$. This is compared to a value of $0.664(4) \text{ s}^{-1}$ found by the commonly used method of zero-trap depth extrapolation, a 2.8% correction that is a result of our model fully taking ensemble loss and heating into account. Finally, we report a five-fold increase in the precision of our collision rate extraction from the experimental data.

I. INTRODUCTION

In a vacuum, single particles or ensembles of single particles are constantly perturbed by collisions with atoms and molecules in the residual background vapor. Energetic elastic and inelastic collisions can result in neutral particle loss from traps [2–5] and ion replacement in ion traps [6]. Collisions that do not impart enough energy to free a trapped particle also constitute an important decoherence mechanism. These collisions can induce heating in neutral ensembles [7–10], melting of ion Coulomb crystals [11–13], reordering of ion chains [14, 15], decoherence in trapped-atom [16] and trapped-ion optical atomic clocks [17], and localization-induced decoherence of single levitated nanoparticles [18, 19]. Understanding the nature of these collisions is important for both producing cold particle ensembles and using them in quantum sensing and quantum information applications.

While understanding the qualitative role of neutral atom loss and ensemble heating due to collisions with the residual background vapor was important for achieving Bose-Einstein condensation in alkali metal gases [9, 20], a rigorous and quantitative understanding of the two effects is essential for the emerging field of quantum vacuum metrology. Here, precise measurements of a sensor particle’s collision rate $\Gamma = n\langle\sigma(v)v\rangle$ can be used with knowledge of the thermally-averaged, velocity-weighted collision cross section $\langle\sigma(v)v\rangle$ to determine the background particle density n [21, 22]. Previous measurements of sensor atom collision rates were conducted by observing the sensor-atom loss rate from shallow magnetic [1, 23–33] and optical dipole traps [34, 35]. As illustrated in Figure 1, the challenge with

this approach lies in the fact that even for exceedingly small trap depths, not every collision results in loss [23, 24]. This complicates extracting the particle’s collision rate from the observed trap loss rate as the instantaneous loss rate varies in time due to its energy dependence. Indeed, both the instantaneous loss rate and heating rate depend on the maximum trap depth (defined for an atom with zero energy) and on the energy distribution of the sensor atoms in the trap. Collisions that do not eject sensor atoms change (heat) the energy distribution of the sensor ensemble, causing the effective trap depth and corresponding loss rate to vary with time. This means that a simple exponential loss model does not adequately capture the behavior of trap loss. Furthermore, as shown here, extrapolation of this loss rate to zero trap depth to obtain the total collision rate relies on data with very low signal-to-noise ratio (SNR), because low trap depth measurements requires culling high energy atoms. These measurements subsequently have a large uncertainty on the total collision rate. This problem cannot be corrected by using higher trap depth measurements, because the variation in the loss rate sharply decreases at small trap depths. This flattening of the loss rate curve cannot be observed at larger trap depths, which makes interpolation from large trap depth inaccurate. Our recent work has accounted for the role of the sensor-atom energy distribution and has added heating corrections to loss rate measurements [29, 30, 32]; however, a more complete description requires an analysis of how the trapped particle energy distribution evolves in time due to these collisions.

In this work, we present a comprehensive theoretical treatment of trapped particle loss and heating due to collisions with a room-temperature background vapor [36]. We derive an analytic expression for the trapped par-

ticle energy distribution evolution in time, based solely on a measured ensemble energy distribution (as the initial condition), the total collision rate, and the probability distribution function $P_t(E)$ for the energy transferred in a collision. Our treatment differs from prior work on the trap depth dependence of ensemble heating rates [7, 8, 29, 30, 32] in that it is valid for all time and for any initial energy distribution. Moreover, it does not rely on a particular form for the transferred energy distribution. We present a direct comparison of the theory with experimental measurements of a magnetically trapped rubidium-87 ensemble exposed to a background vapor of argon. By analyzing the energy evolution of the particles in the trap, we determine the total collision rate with a precision of better than 0.2%. This represents a significant improvement (more than a factor of 5) in the precision for the total collision rate determination. Our theory was recently applied in Ref. [37] to correct the total collision rate reported in a comparison between two cold atom vacuum standards and a classical vacuum metrology apparatus [33].

II. EVOLUTION MODEL

We consider an ensemble of non-interacting particles with mass m subject to a spatially dependent trap potential U . A particle with initial energy E_i and momentum \mathbf{p}_0 , subject to k collisions which transfer momenta $\mathbf{p}_1, \dots, \mathbf{p}_k$ to the particle respectively, will have a final energy E_f given by:

$$E_f = E_i + \sum_{k=1}^n \left(E_k + \frac{\mathbf{p}_k}{m} \cdot \sum_{i=0}^{k-1} \mathbf{p}_i \right) \quad (1)$$

where $E_k = p_k^2/2m$. Details are shown in Appendix A. Since the probability of a collision event is independent of the number of previous collisions undergone by the particle, we model the collisions as Poissonian events that occur with a constant collision rate Γ . The fraction ρ_k of the ensemble that will have undergone k collisions in a time t is then:

$$\rho_k(\Gamma t) = \frac{(\Gamma t)^k e^{-\Gamma t}}{k!} \quad (2)$$

The energy distribution of the ensemble $f(E, t)$ at time t will be the sum of the energy distributions $f_k(E)$ corresponding to the subset of particles that underwent exactly k collisions weighted by the Poissonian probability that k collision events occurred. We can write this as: [36]

$$f(E, t) = \sum_{k=0}^{\infty} \frac{(\Gamma t)^k e^{-\Gamma t}}{k!} f_k(E) \quad (3)$$

The distribution $f_k(E)$ can be computed using the initial energy distribution $f_0(E)$ and the probability

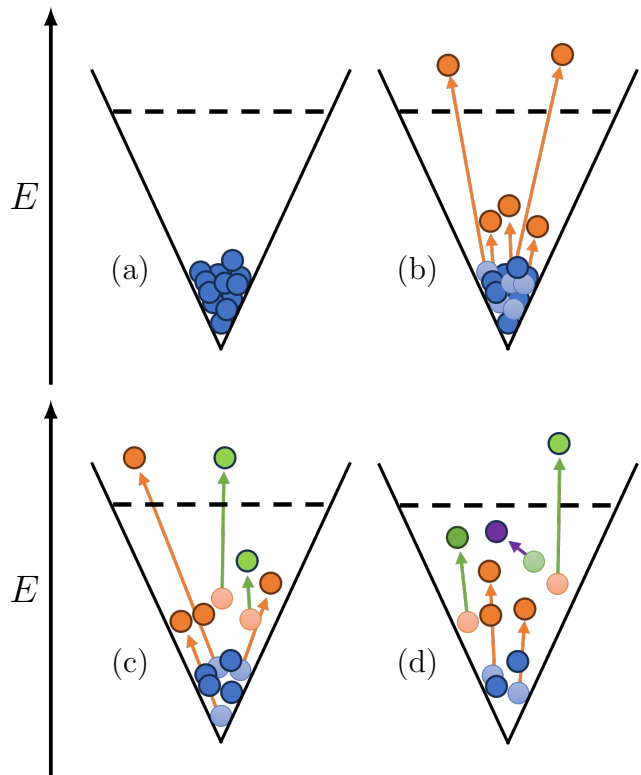


FIG. 1. A schematic showing how background collisions cause the trapped energy ensemble to evolve. The vertical axis denotes energy and the horizontal axis is spatial position in a linear trap potential; however, the form of the confining potential is irrelevant to the analysis presented. The dashed horizontal line demarcates the maximum trap depth E_m . (a) Upon loading in the trap, all of the particles (blue circles) have a low energy and have not undergone any collisions with the background. (b) At short times, some of the particles (light blue circles) have undergone a single collision, which causes them to go to a new state (orange circles). Particles with a new energy larger than E_m are lost. Those with less remain in the trap, but with a higher energy than before – the ensemble has heated. (c) At longer times, particles continue to undergo collisions from a zero to one collision state and also from a one to two collision state (green circles). The one collision particles have a higher energy than they had at the initial time, leading to a higher loss rate. (d) At long times, the energy distribution bears very little similarity to the initial distribution. More particles are in collided states than in initial states, and there are some particles that have undergone three collisions (purple solid circles). These particles can have an energy very close to E_m , and thus have a very small probability of being retained after a fourth collision. This allows the truncation of our analysis after a few collision orders.

$P_t(E)$ that a collision transfers an energy E . Since the incident velocities of the background particles are isotropic, the momentum imparted by the collisions is also isotropic. Then, if we average over the ensemble of particles at a certain energy, the contribution of the cross-term $\mathbf{p} \cdot \mathbf{p}_t/m$ appearing in Eq. 1 will vanish. Hav-

ing appropriate cross-terms such that $E_f < E_i$ is the only way we can have a collision that cools the trapped particle, so we do not need to consider such collisions here. Explicitly, this means that $P_t(E)$ vanishes for $E < 0$. We can therefore perform k convolutions of $f_0(E)$ with $P_t(E)$ for all positive energies to find the distribution $f_k(E)$:

$$f_k(E) = \int_0^\infty dE_1 P_t(E - E_1) \quad (4)$$

$$\times \prod_{j=2}^k \left(\int_0^\infty dE_j P_t(E_{j-1} - E_j) \right) f_0(E_k)$$

where $P_t(E < 0) = 0$ and the product denotes iterated integrals. Substituting this into our expression for the full distribution, we have:

$$f(E, t) = \sum_{k=0}^{\infty} \frac{(\Gamma t)^k e^{-\Gamma t}}{k!} \int_0^\infty dE_1 P_t(E - E_1) \quad (5)$$

$$\times \prod_{j=2}^k \left(\int_0^\infty dE_j P_t(E_{j-1} - E_j) \right) f_0(E_k)$$

Sample plots showing how the total energy distribution and the populations of the $f_k(E)$ distributions change in time are shown in Fig. 2.

In traps of finite depth, particles above some energy U are not trapped, and all collisions that increase the energy above this trap depth result in loss. In this case, we only convolve the distributions up to the energy U , so the previous expression becomes:

$$f(E, t) = \Theta(U - E) \sum_{k=0}^{\infty} \frac{(\Gamma t)^k e^{-\Gamma t}}{k!} \int_0^U dE_1 P_t(E - E_1) \quad (6)$$

$$\times \prod_{j=2}^k \left(\int_0^U dE_j P_t(E_{j-1} - E_j) \right) f_0(E_k)$$

Because $P_t(E)$ does not necessarily vanish for $E > U$, the convolution up to U does not result in a normalized distribution. This reflects loss from the trap; particles that are transferred an energy greater than the trap depth will be lost from the trap and will not appear in experimentally measured energy distributions. We therefore see that this expression provides the trapped particle energy distribution accounting for both heating and loss.

III. THE ENERGY TRANSFER DISTRIBUTION

We now discuss the energy transfer probability distribution from a thermal background to a trapped particle assuming elastic scattering. We will neglect inelastic collisions in the transferred energy distribution, because we

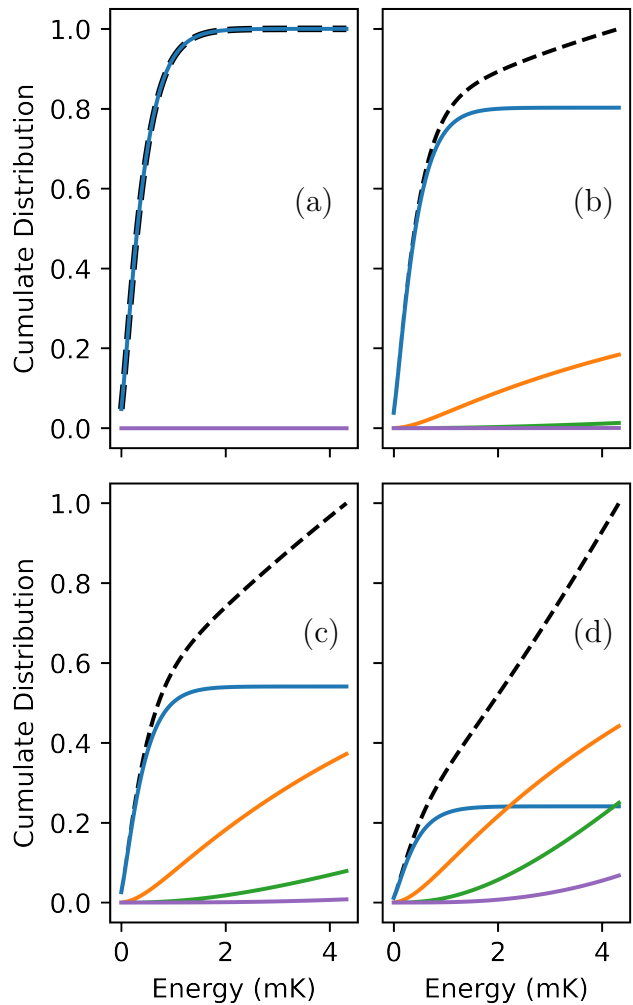


FIG. 2. Cumulative energy distributions for the collision sub-ensembles. We plot the Poisson probability weighted cumulative energy distributions of the k -collision sub-ensembles $f_k(E)$ calculated using Eqn. 4 at different times. Our initial distribution is a Maxwell-Boltzmann distribution for an ^{87}Rb gas at $T = 300 \mu\text{K}$, and we use the transfer energy distribution for the $^{87}\text{Rb} + \text{Ar}$ interaction discussed in Section III. (a) At $\Gamma t = 0$, the total distribution (dashed black) is equal to the initial distribution $f_0(E)$ (blue) because the ensemble has not yet undergone collisions. (b) At $\Gamma t = 1$, the ensemble is still dominated by $f_0(E)$, but there is also a small contribution from $f_1(E)$ (orange) and a much smaller contribution from $f_2(E)$ (green). We see the shape of the total distribution as a result of these new contributions. (c) At $\Gamma t = 3$, there are a similar number of particles in the $f_0(E)$ and $f_1(E)$ sub-ensembles. The contribution of the $f_2(E)$ has increased, and $f_3(E)$ (purple) is nonzero. (d) At $\Gamma t = 8$, the distribution is now dominated by the $f_1(E)$ sub-ensemble, and $f_0(E)$ and $f_2(E)$ have approximately equal populations. The total distribution has now changed significantly from the initial distribution, and only reflects $f_0(E)$ in the small energy regime.

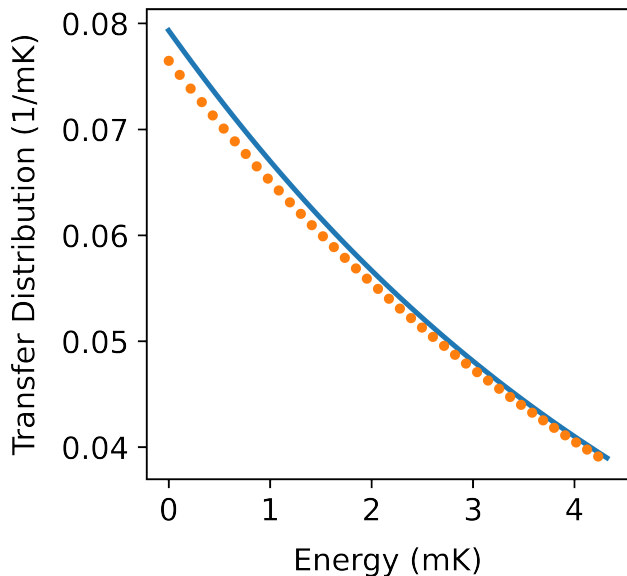


FIG. 3. The transfer energy distribution, $P_t(E)$ for rubidium-87 atoms subject to collisions by argon atoms at room temperature. The solid blue line is $P_t(E)$ obtained from Eqn. 11 using the scattering amplitudes computed by quantum scattering calculations as input. The orange dotted line is obtained by differentiating the trap depth dependent loss rate based on quantum diffractive universality (shown in Eqn. 13) with parameters found in Ref [29]. These distributions are not normalized over the range of energies shown, reflecting the fact that collisions can cause loss. The two curves are very similar; the largest deviation between the two is 3.6%, and the cumulate difference between the them is 2.28%. As we discuss in Section IV, the total collision rate extracted using these two different $P_t(E)$ curves differ by 0.61%. Since the quantum scattering calculations require significant computational resources, it may be more convenient and sufficiently accurate to simply use the universal polynomial.

assume that all inelastic collisions generate trap loss. We discuss two methods for finding $P_t(E)$. The first method is to compute it from first principles using interaction potentials and quantum scattering calculations. The second method is to use a prediction based on quantum diffractive universality, under which interactions between the trapped and background species that are sufficiently dominated by a long range van-der Waals type interaction follow a universal trap depth dependent loss function [1, 28].

A. Transfer probability from quantum scattering calculations

We consider a trapped particle of mass m_t and velocity \mathbf{v}_t subject to an incident background particle of mass m_b and velocity \mathbf{v}_b . We can reduce the analysis of the collision to the case of single incident particle in the center of mass frame with reduced mass $\mu = m_t m_b / (m_t + m_b)$

and velocity $\mathbf{v} = \mathbf{v}_t - \mathbf{v}_b$ subject to the interaction potential. Consider such a particle in the plane-wave state $|\mathbf{k}\rangle$ with an initial momentum $\hbar\mathbf{k}$. The probability amplitude of the particle transitioning into a state $|\mathbf{k}'\rangle$ with momentum $\hbar\mathbf{k}'$ is given by the scattering amplitude $\mathcal{F}(\mathbf{k}, \mathbf{k}')$. Because we are in the center of mass frame, this amplitude is only nonzero if $|\mathbf{k}| = |\mathbf{k}'|$.

We assume that the potential energy surface of the interaction potential is spherically symmetric. In this case, the scattering amplitude must also be rotationally invariant, and it can be written as:

$$\mathcal{F}(\mathbf{k}, \mathbf{k}') = \sum_{\ell=0}^{\infty} (2\ell + 1) \mathcal{F}_{\ell}(k) P_{\ell}(\cos \theta) \quad (7)$$

where θ is the angle between \mathbf{k} and \mathbf{k}' , P_{ℓ} are the Legendre polynomials, and the partial wave amplitudes \mathcal{F}_{ℓ} are functions we must compute. We can re-write the scattering amplitudes as functions of the incoming velocity of the background particle and the scattering angle as:

$$\mathcal{F}_v(\theta) = \sum_{\ell=0}^{\infty} (2\ell + 1) \mathcal{F}_{\ell}(v/\mu\hbar) P_{\ell}(\cos \theta) \quad (8)$$

The probability \mathcal{P}_v that a particle with velocity v transfers an energy E is given by the probability that the particle scatters at a relative angle θ corresponding to that energy normalized by the total probability that the collision occurs. This normalization constant is the total velocity cross-section $\sigma(v)$. As calculated in Appendix B, the energy transferred by an incident particle of relative velocity v that scatters with an angle θ is given by:

$$E_t = \frac{2\mu^2 v^2}{m} \sin^2\left(\frac{\theta}{2}\right) \quad (9)$$

Using this, we can write \mathcal{P}_v as:

$$\mathcal{P}_v(E) = \frac{|\mathcal{F}_v(\theta)|^2}{\sigma(v)} \delta\left(E - \frac{2\mu^2 v^2}{m} \sin^2\left(\frac{\theta}{2}\right)\right) \quad (10)$$

To convert this into the ensemble energy transfer distribution, we must average over the relative velocity distribution. As shown in Appendix C, this can be very well approximated by the Maxwell Boltzmann distribution that describes the background gas in the rest frame. We also account for the difference in the fluxes in the background gas by adding a velocity weight. Furthermore, the probability of a collision occurring depends on the velocity, so we must also add a velocity cross-section weighting which cancels out with the velocity cross-section in the denominator of Eqn. 10. We normalize by the total ensemble averaged velocity-weighted

cross-section to ensure unit probability when the distribution is integrated over all energies. This gives us the expression:

$$P_t(E) = \frac{4\pi}{\langle \sigma(v)v \rangle} \left(\frac{m_b}{2\pi k_B T} \right)^{3/2} \int_0^\infty dv \int_0^\pi d\theta \sin\theta \quad (11)$$

$$\times v^3 e^{-m_b v^2/2k_B T} |\mathcal{F}_v(\theta)|^2 \delta \left(E - \frac{2\mu^2 v^2}{m} \sin^2 \left(\frac{\theta}{2} \right) \right)$$

To find the energy transfer distribution function $P_t(E)$, for our comparison with measurements of a ^{87}Rb sensor ensemble exposed to an Ar gas, we first calculated the scattering amplitudes $\mathcal{F}_v(\theta)$ using the interaction potential for Rb+Ar from Ref. [38] as input to a single channel quantum scattering computation as described in Ref. [1]. We then used these values as input to Eqn. 11 to find $P_t(E)$. The results are shown in Figure 3.

B. Transfer probability from quantum diffractive universality

Another approach to finding the energy transfer distribution function is to use the universality predictions of Refs. [1, 28]. There, it was shown that the loss rate Γ_ℓ of a particle with zero initial energy as a function of the trap depth U normalized to the total collision rate Γ , can be described by:

$$\frac{\Gamma_\ell(U)}{\Gamma} = 1 - \sum_{k=1}^{\infty} \beta_k \left(\frac{U}{U_d} \right)^k \quad (12)$$

where the β_k are species-independent coefficients and U_d is a species-dependent quantum diffraction energy scale. The values of the coefficients for the first six terms and the experimentally measured values of U_d for ^{87}Rb subject to various background species can be found in Refs. [1, 28].

If the trapped ensemble distribution is localized to a single energy, the normalized loss rate is the probability that a collision will transfer an energy greater than U . In other words, it is the complement of the cumulative energy transfer distribution. Thus, we can obtain $P_t(E)$ by differentiating Eqn. 12, which yields:

$$P_t(E) = \frac{1}{U_d} \sum_{k=0}^{\infty} (k+1) \beta_{k+1} \left(\frac{U}{U_d} \right)^k \quad (13)$$

This expression is easy to evaluate, and, as shown in Figure 3, the β_k and U_d values taken from Refs. [1, 28] provide a good approximation to the transfer distribution found using a quantum scattering calculation for Rb+Ar collisions.

IV. EXPERIMENTAL MEASUREMENT

The experimental apparatus used in this study is described in Ref. [1]. Briefly, it consists of a Rb source, a two-dimensional (2D) magneto-optical trap (MOT) section, a three-dimensional (3D) MOT section, and a pump section. The experiment procedure begins by loading Rb atoms into the 2D MOT from the Rb vapor generated by the atom source. A laser beam aligned to the center of the 2D MOT pushes atoms through a differential pumping tube into the 3D MOT region where they accumulate. The magnetic field configuration of the 3D MOT is a spherical quadrupole and is operated with an axial gradient of 13.6 G/cm along the vertical direction. In both the 2D MOT and 3D MOT, the trapping lasers are detuned 12 MHz below the ^{87}Rb $5^2S_{1/2} \rightarrow 6^2P_{3/2}, F = 2 - 3'$ transition, and the ‘repump’ lasers are tuned on resonance with the $5^2S_{1/2} \rightarrow 5^2P_{3/2}, F = 1 - 2'$ transition. After the particles are loaded into the 3D MOT, the pump laser frequency is detuned to 60 MHz below the $F = 2 \rightarrow F = 3$ transition for 50 ms to further cool the atom ensemble. Next, the atoms are optically pumped to the $F = 1$ hyperfine ground state by shutting off the repump laser and leaving the pump laser on for another 4 ms. Then, we extinguish the pump laser and ramp up the magnetic field axial gradient to 272 G/cm in 10 ms. Only atoms in the low-field seeking state, $|F = 1, m_F = -1\rangle$ are confined in the magnetic trap (MT). The atoms are held in the MT for a time t before being recaptured in the MOT using the same detunings during the stage just before hyperfine pumping. To count the atom number, we image the MOT ensemble fluorescence onto a photodetector inducing a voltage, V , that is proportional to the atom number, N . The fraction of atoms in the MT recaptured in the MOT is found by dividing the recaptured atomic fluorescence $V_{\text{MT}}(t)$ by the initial MOT fluorescence V_{MOT} :

$$R(t) = \frac{V_{\text{MT}}(t)}{V_{\text{MOT}}} \quad (14)$$

To set the magnetic trap depth for the atom ensemble, an RF field is applied at the end of the hold time. The RF field induces transitions of the atoms from the trapped state ($|F = 1, m_F = -1\rangle$) to the $|F = 1, m_F = 0, +1\rangle$ states that are not trapped by the MT. During the RF radiation phase, the RF frequency is swept between ν_{min} and ν_{max} . Atoms with the magnetic energies above $E_m = \hbar\nu_{\text{min}}$ encounter a resonant RF field and are flipped into an untrappable spin state and escape from the trap. We therefore define E_m to be the maximum trap depth. The RF radiation is swept sufficiently for a sufficiently long time in comparison to the motion of the particles in the trap to ensure that every particle which reaches the magnetic energy E_m during their motion will encounter the RF field. As a result, all particles that achieve a maximum magnetic energy of E_m or higher during their evolution are ejected.

It should be noted that the maximum magnetic energy achieved by the particles is not necessarily the total energy of the particle. Through the course of a particle's trajectories, its energy is divided between magnetic potential energy, gravitational potential energy, and kinetic energy. It is possible that at the time where the particle reaches its maximum magnetic energy, it has nonzero gravitational and kinetic energies. However, in the limit of large magnetic field gradients, these energies will be negligible relative to the magnetic energy. We therefore conduct our experiments at a gradient that is sufficiently high such that the maximum magnetic energy of the particle is essentially the same as the total energy of the particle. This limit is reached when the trapping gradient is much larger than the minimum gradient required to magnetically levitate the atoms and when the initial kinetic energy of the atoms (set by the MOT) is much smaller than their magnetic potential energy set by the initial cloud size and the MT gradient. The study of the relationship between the total energy and the maximum magnetic energy outside of this limit is beyond the scope of this work and is the topic of future work.

To measure the time-dependent cumulative energy distribution function (CDF), $F(E_m, t) = \int_0^{E_m} f(E, t) dE$, of the atoms in the magnetic trap, we measure the fraction $R(t)$ of atoms in the magnetic trap that are recaptured in the MOT after the hold time t as a function of the trap depth E_m . To observe the time evolution of the cumulative energy distribution, we repeat the CDF measurement for a series of hold times t_1, \dots, t_k . The measured time-dependent CDFs are presented as discrete dots in Fig. 4.

V. VALIDATION OF THE MODEL

For the comparison of the theoretical model and experiment, we flow pure Ar gas into the experiment chamber through the pump section in the apparatus. We maintain the Ar pressure at 10^{-6} Pa, which is two orders of magnitude higher than the initial ambient gas pressure. Therefore, we can approximate the entirety of the background to be Ar gas.

Since our experimental measurements are of the CDF of the trapped ensemble, we integrate Eq. 6 to find the time-dependent cumulative energy distribution F of the trapped ensemble:

$$F(E, t) = \int_0^E dE_0 \Theta(U - E_0) \sum_{k=0}^{\infty} \frac{(\Gamma t)^k e^{-\Gamma t}}{k!} \times \prod_{j=1}^k \left(\int_0^U dE_j P_t(E_{j-1} - E_j) \right) f_0(E_k) \quad (15)$$

where U is the maximum possible energy a trapped particle can have. To make the comparison, we must first measure the initial distribution $f_0(E)$ at time t_0 , then evaluate the expression for $F(E, t)$ and compare it to the experimentally measured recapture fractions $R(E, t + t_0)$ at various hold times. The only free parameter in our procedure is the total collision rate Γ , which is determined from the observed loss rate and the ensemble distribution changes. This method provides a much more precise determination of the total collision rate than the method previously used – an extrapolation of the exponential decay fits back to zero trap depth.

One challenge with the proposed procedure is finding the initial energy distribution. We experimentally measure CDFs, but our model uses its derivative, the probability density function (PDF) $f_0(E)$. When the CDF measurements are differentiated, the underlying measurement noise can lead to un-physical (negative values) and jagged features in the PDF. We resolved this issue by using Gaussian Process Regression (GPR) to calculate a smooth function to describe the CDF data with the constraint that the resultant CDF be monotonically increasing. This gives us a smooth, positive-definite probability distribution. We used the gpytorch Gaussian process (GP) library provided by Ref. [39]. To account for the uncertainty in the experimental measurements, we re-sampled each experimental data point used to calculate the loss in each iteration of the algorithm from a Gaussian distribution centered on the measurement with a standard deviation equal to the uncertainty of the measurement. This has the added benefit of combining the fitting uncertainty and experimental uncertainty for the initial distribution that can be used for measurement uncertainty analysis. The results of the GP interpolations to all of the experimental CDFs are shown in Fig. 4.

Using the shortest hold time ($t_0 = 0.7$ seconds) CDF interpolation shown in Fig. 4 as the initial distribution, we used Eqn. 15 to numerically calculate the CDF predicted by the model for different times $t = t_e - t_0$, where the t_e are the run times of the experimental data. We evaluated the series in Eqn. 15 up to the fourth order heating term, which has a contribution of less than 0.1% for the time scales considered. Higher order terms are even smaller and were neglected.

Given $f_0(E)$ and $P_t(E)$, the only free parameter remaining in the model is Γ , the total collision rate. To find it, we perform a global mean square error fit. Namely, we use Eq. 15 to compute the predicted CDFs and then evaluate the global sum of the squared residuals between all of the CDFs calculated by the model and the experimental CDFs. To account for the measurement uncertainty in the experimental points, we sample each experimental data comparison point from a Gaussian distribution centered on the GPR interpolated curves (shown in Fig. 4) with a standard deviation equal to the standard deviation

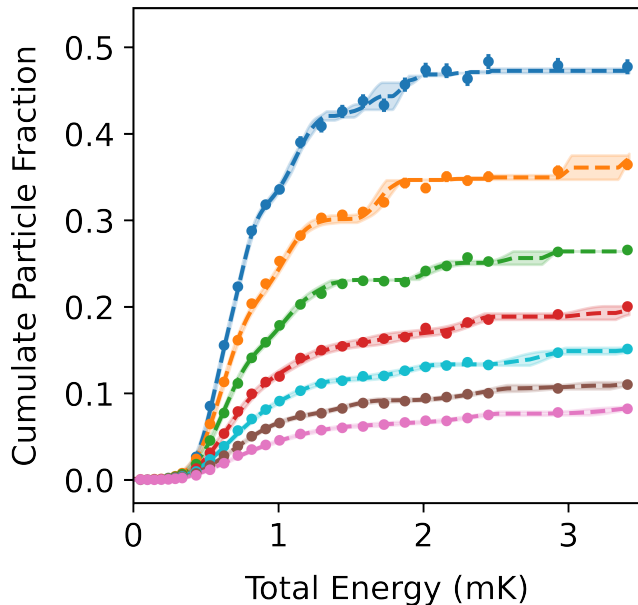


FIG. 4. Experimental and interpolated cumulative energy distributions of an ^{87}Rb atomic ensemble in a magnetic trap after different hold times to a background gas of Ar. The ensemble lifetime was approximately 1.5 seconds and the hold times were 0.7 s (blue), 1.2 s (orange), 1.8 s (green), 2.3 s (red), 2.8 s (cyan), 3.4 s (brown), and 3.9 s (pink). Experimentally measured values (dots) and Gaussian Process Regression (GPR) interpolations (lines) are shown with shaded regions that indicate the combined uncertainties in the GPR interpolation and the experimental data. To achieve this, between every iteration of the GPR, we re-sampled each data point against which the GPR interpolation curve is compared from a Gaussian distribution centered on the measured value with standard deviation equal to the uncertainty in the measurement.

tion of the interpolation at this point. We then find the value of Γ that minimizes the global sum of the squared residuals. This final minimization step is repeated for 200 different sample sets providing 200 distinct values of Γ . The mean of these values is our reported Γ , and the standard deviation tells us the propagation of the measurement uncertainty into our value of the collision rate. The fit uncertainty for each sample set is several orders of magnitude smaller than the variation of the Γ values arising from the measurement uncertainty, so we do not consider it. We find a collision rate of $\Gamma = 0.646(1) \text{ s}^{-1}$, which is 10.8% higher than what would be obtained by fitting the highest energy points in the CDFs to an exponential decay law and is 2.8% higher than the result obtained by extrapolating the loss rates to zero trap depth. A plot of the model CDF fits with this value of the collision rate compared to the experimental data is shown in Figure 5. The uncertainty $\Delta\Gamma \approx 1.5 \times 10^{-4}\Gamma$, which an improvement in precision from our previous analysis methods by over a factor of five. We note that this increase in precision is not due to using the GPR inter-

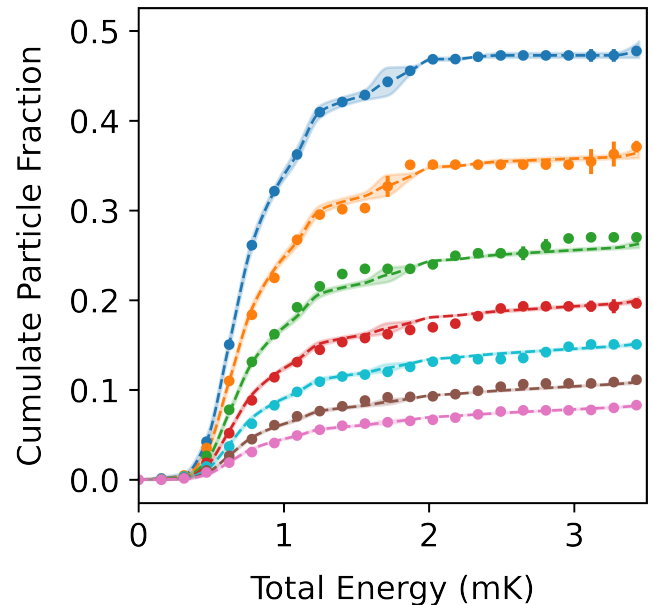


FIG. 5. Experimental and model-predicted cumulative particle energy distributions at different times. The points are experimental data (the same as in Fig. 4), and the solid lines are the distributions predicted by the model (Eqn. 15). The shaded region is the uncertainty in the model that propagates from the uncertainty in the initial distribution. The highest particle number curve (blue) was taken at the experimental hold time $t_0 = 0.7$ s, and it is used as an initial distribution for the model. The subsequent curves are obtained by evaluating the model at times $t = t_e - t_0$, where t_e is the experimental hold time used for the corresponding CDF. The values of t_e for the curves shown here are 1.2 s (orange), 1.8 s (green), 2.3 s (red), 2.8 s (cyan), 3.4 s (brown), and 3.9 s (pink). The fit of the model to the experimental data provides the collision rate. We find a value of $\Gamma = 0.646(1) \text{ s}^{-1}$. By construction, we have perfect agreement between the experiment and model at $t = 0$, but we see that the curves agree for longer hold times as well.

polation to increase our sample size to which we can fit. The fitting of the model to the GPR interpolated data uses fewer points than actually gathered in the experiment, demonstrating that the precision is a product of the method and not the sample size.

VI. CONCLUSION

We have presented a mathematically rigorous model for the time evolution of the energy distribution of a trapped particle ensemble as a result of collisions with a thermal background gas. We have also described an analysis method that allows us to compare cumulative distributions functions predicted by our model to experimental data. This procedure involves finding the collision-induced transfer energy distribution, using a Gaussian process regression to interpolate the data,

and performing a single-parameter fit that extracts the collision rate. We have used this procedure and found good agreement between our model and experimental data obtained for trapped ^{87}Rb subject to a thermal argon background. We obtained a total collision rate, using information about heating and trap loss, of $0.646(1) \text{ s}^{-1}$. This is an uncertainty of below 0.2%, which is significantly more precise than any previous measurements.

This work has several implications for future studies in the area of particle sensors for vacuum metrology. Our work suggests that previous collision rate measurements need to be corrected to account for the change in the distribution, and we have presented a theory to perform this correction that provides the total collision rate with a low uncertainty. This theory is presently being applied to reanalyze both our previous measurements (Refs. [1, 28, 29]) and measurements taken by other groups [37]. We note that this theory can be applied to other species (e.g. molecules), trap geometries, and experimental procedures, as it does not depend on the distribution of the particles loaded into the trap or the trapping potential that is used. It only depends on one CDF measurement used as an initial distribution f_0 to evolve and knowledge of the transfer energy distribution; no additional information about the experimental details are required. We further comment that our method is robust against noise in the measurement of f_0 and prior heating that has already changed f_0 from the distribution first loaded into the trap. We can also generalize the evolution model to systems with multiple background particles by adding an additional set of iterated integrals for each species present.

The analysis techniques we have discussed provides new ways to understand and study diffractive collision physics. In particular, our formulation of the cumulative distribution functions in Eqn. 15 suggests a way to measure the transfer distribution using experimental data. As a preliminary test, we found that repeating the analysis described in Section III using the universal polynomial form of the transfer distribution shown in Eqn. 13 yields a total collision rate of $0.642(1) \text{ s}^{-1}$. This differs by our result computed for the Medvedev transfer function by 0.61%, demonstrating the effectiveness of quantum diffractive universality in describing the low energy sector of the transfer energy distribution for $^{87}\text{Rb}+\text{Ar}$ collisions. We intend to extend this analysis to other species and refine our understanding of the uses and limits of universality [1].

VII. APPENDIX

A. Single Particle Heating

In this section, we show our derivation of the energy transferred to a trapped particle after k -collisions as shown in Eqn. 1. We consider a cold trapped gas of particle mass m in a quadrupole trap subject to the potential U that is only a function of the coordinate \mathbf{x} . We subject the trapped gas to a background thermal gas of particle mass m_b . Consider a trapped particle with momentum \mathbf{p} at a position \mathbf{x} that collides with a background particle of mass m_b , and let \mathbf{p}_t be the momentum transferred to the trapped particle by the collision. The final energy E_f of the particle will be:

$$E_f = \frac{(\mathbf{p} + \mathbf{p}_t)^2}{2m} + U(\mathbf{x}) \quad (16)$$

We now define the transfer energy E_t to be:

$$E_t = \frac{p_t^2}{2m} \quad (17)$$

We can rewrite the final energy in terms of the initial energy E_i and the transfer energy in the following way:

$$E_f = E_i + E_t + \frac{\mathbf{p} \cdot \mathbf{p}_t}{m} \quad (18)$$

Next, suppose that the particle with momentum \mathbf{p}_0 undergoes n collisions with transfer momenta $\mathbf{p}_1, \dots, \mathbf{p}_n$. Apply induction to Equation 18 tells us that the final energy E_f of the particle is given by:

$$E_f = E_i + \sum_{k=1}^n \left(E_k + \frac{\mathbf{p}_k}{m} \cdot \sum_{i=0}^{k-1} \mathbf{p}_i \right) \quad (19)$$

B. Single Particle Energy Transfer

Here, we shall calculate how the energy transferred in a collision event depends on the relative velocities of the particles and the scattering angle as shown in Eqn. 9. Suppose that the background particle has incoming momentum \mathbf{p}_i in the rest frame of the trapped particle, that the background particle scatters with outgoing momentum \mathbf{p}_f , and the trapped particle scatters with outgoing momentum \mathbf{q}_f . The conservation of momentum tells us that:

$$\mathbf{p}_i = \mathbf{p}_f + \mathbf{q}_f \quad (20)$$

As the trapped particle is initially stationary, the center of mass velocity \mathbf{v}_c is given by:

$$\mathbf{v}_c = \frac{\mathbf{p}_i}{m + m_b} \quad (21)$$

We can boost into the center of mass frame through the Galilean transformation $\mathbf{v} \mapsto \mathbf{v} - \mathbf{v}_c$. Let \mathbf{p}'_i and \mathbf{p}'_f

denote the initial and final momenta of the background particle in the center of mass frame and let \mathbf{q}'_i and \mathbf{q}'_f denote the initial and final momenta of the trapped particle in the center of mass frame. By definition, we know that:

$$\mathbf{p}'_i = \mathbf{p}_i - m_b \mathbf{v}_c \quad (22)$$

Substituting in our expression for \mathbf{v}_c and simplifying, we find:

$$\mathbf{p}'_i = \frac{m\mathbf{p}_i}{m + m_b} \quad (23)$$

The conservation of energy tells us that:

$$\frac{q_i'^2}{2m} + \frac{p_i'^2}{2m_b} = \frac{q_f'^2}{2m} + \frac{p_f'^2}{2m_b} \quad (24)$$

In the center of mass frame, the total momentum of the system vanishes. Thus, $\mathbf{p}'_i = -\mathbf{q}'_i$ and $\mathbf{p}'_f = -\mathbf{q}'_f$. Substituting these results into our expression for the conservation of energy, we have:

$$\frac{p_i'^2}{2m} + \frac{p_i'^2}{2m_b} = \frac{q_f'^2}{2m} + \frac{q_f'^2}{2m_b} \implies p_i' = q_f' \quad (25)$$

This tells us that \mathbf{q}'_f is equal to \mathbf{p}'_i up to some rotation. We can now choose our coordinates such that \mathbf{p}_i lies along the x -axis and \mathbf{q}_f lies in the xy -plane. Then, \mathbf{p}'_i lies along the x -axis and \mathbf{q}'_f is also in the xy -plane. Let θ be the angle between \mathbf{p}'_i and \mathbf{p}'_f . As \mathbf{p}'_f and \mathbf{q}'_f have opposite directions, the angle between \mathbf{p}'_i and \mathbf{q}'_f will be $\theta + \pi$. We can summarize these relationships in terms of a rotation matrix in the following way:

$$\mathbf{q}_f = \begin{pmatrix} \cos(\pi + \theta) & -\sin(\pi + \theta) \\ \sin(\theta + \pi) & \cos(\theta + \pi) \end{pmatrix} \mathbf{p}'_i + m\mathbf{v}_c \quad (26)$$

We can write \mathbf{p}'_i and \mathbf{v}_c in terms of \mathbf{p}_i , which yields:

$$\mathbf{q}_f = \begin{pmatrix} -\cos\theta & \sin\theta \\ -\sin\theta & -\cos\theta \end{pmatrix} \frac{m\mathbf{p}_i}{m + m_b} + \frac{m\mathbf{p}_i}{m + m_b} \quad (27)$$

In these coordinates, \mathbf{p}_i lies along the x -axis. Then, this expression becomes:

$$\mathbf{q}_f = \frac{mp_i}{m + m_b} \begin{pmatrix} 1 - \cos\theta \\ -\sin\theta \end{pmatrix} \quad (28)$$

The energy E_t transferred to the trapped particle in the frame where it is at rest is merely the final kinetic energy of the particle, which is $q_f^2/2m$. Then, our previous expression tells us that:

$$E_t = \frac{1}{m} \left(\frac{mp_i}{m + m_b} \right)^2 (1 - \cos\theta) \quad (29)$$

Now, we define the reduced mass of the system μ to be:

$$\mu = \frac{mm_b}{m + m_b} \quad (30)$$

Writing the transfer energy expression in terms of the reduced mass yields:

$$E_t = \frac{2\mu^2 p_i^2}{mm_b^2} \sin^2\left(\frac{\theta}{2}\right) \quad (31)$$

Notice that p_i/m_b is merely the relative velocity of the background particle. We denote this velocity to be v_r . In terms of this velocity, we conclude that:

$$E_t = \frac{2\mu^2 v_r^2}{m} \sin^2\left(\frac{\theta}{2}\right) \quad (32)$$

C. The Background Gas Distribution

In this section, we shall justify our approximation of the relative speed distribution of the background particles using the lab frame speed distribution of the background gas. In the lab frame, the background obeys a Maxwell-Boltzmann velocity distribution $d(v)$ with some temperature T . However, as the trapped particle is not at rest the relative velocity distribution is some other function $d'(v_r)$. Let ϵ be the velocity of the trapped particle. The deviation is maximized when ϵ is collinear with the velocity of incoming background particle, because this maximizes the difference between the magnitudes of the background particle velocity and the relative velocity. We shall then take ϵ to be in the same direction as the background particle velocity, which reduces this to a one dimensional problem. The relative speed distribution d' is:

$$d'(v) = 4\pi \left(\frac{m_b}{2\pi k_B T} \right)^{3/2} (v + \epsilon)^2 e^{-m_b(v+\epsilon)^2/2k_B T} \quad (33)$$

where m_b is the mass of the background particle. Expanding about $\epsilon = 0$, we find:

$$d'(v) = 4\pi \left(\frac{m_b}{2\pi k_B T} \right)^{3/2} v^2 e^{-m_b v^2/2k_B T} \times \left(1 + \frac{2\epsilon}{v} - \frac{m_b v \epsilon}{k_B T} - \frac{5m_b \epsilon^2}{2k_B T} + \dots \right) \quad (34)$$

where we have dropped terms of order ϵ^k/v^k , ϵ^k/T^k and $v^k \epsilon^k/T^k$ for $k \geq 2$. The velocity ϵ is of order $\sqrt{3k_B T_t/m_t}$ where T_t is the trap temperature and m_t is the trapped particle mass. Similarly, v is of order $\sqrt{3k_B T/m_b}$. Then, we can write:

$$\left(1 + \frac{2\epsilon}{v} - \frac{m_b v \epsilon}{k_B T} - \frac{5m_b \epsilon^2}{2k_B T} + \dots \right) \sim \left(1 - \frac{15m_b T_t}{m_t T} - \sqrt{\frac{m_b T_t}{m_t T}} \right) \quad (35)$$

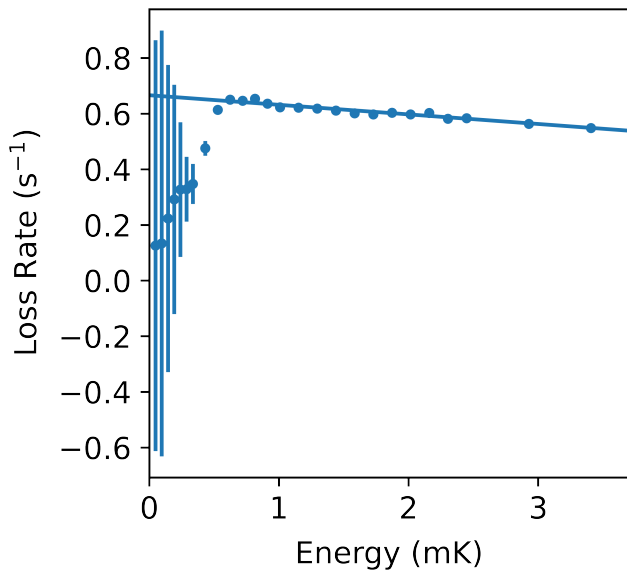


FIG. 6. The ensemble loss rate versus trap depth extracted from the data in Fig. 4. The cumulative particle fraction at a fixed cut energy and different hold times were fit to a simple exponential function to obtain an estimate for the loss rate at different trap depths. These loss rate values were then extrapolated back to find the value at zero trap depth. The extrapolated value is $\Gamma = 0.664(4) \text{ s}^{-1}$ if the values at small depths and with large uncertainties are excluded from the fit. If all points are included, the value is $\Gamma = 0.4(3) \text{ s}^{-1}$.

For our system, $T_t \sim 100 \text{ } \mu\text{K}$, T is 294 K, and $m_b/m_t = 0.46$. Then, the correction is of order 1×10^{-6} .

This analysis is not comprehensive, as the background particle and trapped particle velocities are both drawn from probability distributions that can deviate from the mean value estimates. However, even if we consider $0 \text{ m/s} < \epsilon < 0.47 \text{ m/s}$ and $80 \text{ m/s} < v < 1000 \text{ m/s}$, which includes 99% of sampled ϵ and v , the maximum value that the correction term reaches is 0.011. This also does not account for the fact that the trapped particle velocity is randomly oriented, so the projection of ϵ along \mathbf{v} will be smaller than predicted by the speed distribution.

This justifies our approximation that $d'(v) \approx d(v)$.

D. Extrapolating the loss rate

An alternative approach to the one presented here for obtaining the total collision rate from the observed loss rate is to fit the recaptured fraction as a function of hold time to a simple exponential decay law at progressively smaller and smaller trap depths. The results can then be extrapolated to zero trap depth to infer the total collision rate.

To illustrate the limits of this approach, the ensemble loss rate versus trap depth was extracted from the data in Fig. 4. The cumulative particle fraction at a fixed cut energy and different hold times was fit to a simple exponential function to obtain the loss rate at that trap depth. The results are shown in Fig 6. The resulting loss rates were then extrapolated back to infer the loss rate at zero trap depth. The extrapolated value at zero trap depth is $\Gamma = 0.664(4) \text{ s}^{-1}$ if the values at small trap depth and with large uncertainties are excluded from the fit. This value is larger by 2.8 % than the value extracted from the rigorous analysis of the CDFs.

There are several problems with this naive approach. One is that the ensemble loss rate is not a simple exponential and actually increases with time as the ensemble heats. The second problem is that, because the atoms are not at zero energy, the effective trap depth of the ensemble is not the same as the cut energy at which the CDF is taken. A manifestation of this is that, because the energy distribution of the atoms has a non-zero width and may also include an offset below which there are no atoms, the trap depth dependence of the loss rate becomes flat at the lowest cut energies. Evidently, another consequence of this difference between the cut energy and the effective trap depth is that an overestimate results when extrapolating the trap loss rate back to zero cut energy using only data at higher trap depths where the SNR is high.

[1] J. L. Booth, P. Shen, R. V. Krems, and K. W. Madison, *New Journal of Physics* **21**, 102001 (2019).
 [2] A. L. Migdall, J. V. Prodan, W. D. Phillips, T. H. Bergeman, and H. J. Metcalf, *Phys. Rev. Lett.* **54**, 2596 (1985).
 [3] J. E. Bjorkholm, *Phys. Rev. A* **38**, 1599 (1988).
 [4] B. Hemmerling, G. K. Drayna, E. Chae, A. Ravi, and J. M. Doyle, *New Journal of Physics* **16**, 063070 (2014).
 [5] C. J. Rennick, J. Lam, W. G. Doherty, and T. P. Softley, *Phys. Rev. Lett.* **112**, 023002 (2014).
 [6] P. Obřil, A. Lešundák, T. Pham, K. Lakhmanskiy, L. Podhora, M. Oral, O. Číp, and

L. Slodička, *Review of Scientific Instruments* **90**, 083201 (2019), <https://pubs.aip.org/aip/rsi/article-pdf/doi/10.1063/1.5104346/15884270/083201.1.online.pdf>.
 [7] H. C. W. Beijerinck, *Phys. Rev. A* **61**, 033606 (2000).
 [8] H. C. W. Beijerinck, *Phys. Rev. A* **62**, 063614 (2000).
 [9] E. A. Cornell, J. R. Ensher, and C. E. Wieman, *arXiv:cond-mat/9903109v1* (1999).
 [10] S. Bali, K. M. O'Hara, M. E. Gehm, S. R. Granade, and J. E. Thomas, *Phys. Rev. A* **60**, R29 (1999).
 [11] F. Kranzl, M. K. Joshi, C. Maier, T. Brydges, J. Franke, R. Blatt, and C. F. Roos, *Phys. Rev. A* **105**, 052426 (2022).

- [12] G. Pagano, P. W. Hess, H. B. Kaplan, W. L. Tan, P. Richerme, P. Becker, A. Kyprianidis, J. Zhang, E. Birkelbaw, M. R. Hernandez, Y. Wu, and C. Monroe, *Quantum Science and Technology* **4**, 014004 (2018).
- [13] D. Kiesenhofer, H. Hainzer, A. Zhdanov, P. C. Holz, M. Bock, T. Ollikainen, and C. F. Roos, *PRX Quantum* **4**, 020317 (2023).
- [14] Y. Aikyo, G. Vrijsen, T. W. Noel, A. Kato, M. K. Ivory, and J. Kim, *Applied Physics Letters* **117**, 234002 (2020), <https://pubs.aip.org/aip/apl/article-pdf/doi/10.1063/5.0029236/14543125/234002.1.online.pdf>.
- [15] R. F. Spivey, I. V. Inlek, Z. Jia, S. Crain, K. Sun, J. Kim, G. Vrijsen, C. Fang, C. Fitzgerald, S. Kross, T. Noel, and J. Kim, *IEEE Transactions on Quantum Engineering* **3**, 1 (2022).
- [16] K. Gibble, *Phys. Rev. Lett.* **110**, 180802 (2013).
- [17] A. M. Hankin, E. R. Clements, Y. Huang, S. M. Brewer, J.-S. Chen, C. W. Chou, D. B. Hume, and D. R. Leibbrandt, *Phys. Rev. A* **100**, 033419 (2019).
- [18] L. Magrini, P. Rosenzweig, C. Bach, A. Deutschmann-Olek, S. G. Hofer, S. Hong, N. Kiesel, A. Kugi, and M. Aspelmeyer, *Nature* **595**, 373 (2021).
- [19] M. Aspelmeyer, arXiv:2203.05587 (2023).
- [20] C. R. Monroe, E. A. Cornell, C. A. Sackett, C. J. Myatt, and C. E. Wieman, *Phys. Rev. Lett.* **70**, 414 (1993).
- [21] J. Booth, D. E. Fagnan, B. G. Klappauf, K. W. Madison, and J. Wang, “Method and device for accurately measuring the incident flux of ambient particles in a high or ultra-high vacuum environment,” (2011), uS Patent 8,803,072.
- [22] K. W. Madison, “A cold atom based UHV pressure standard,” personal communication (2012), seminar at the National Institute of Standards and Technology, Gaithersburg, MD, December 4, 2012; seminar at the Laboratoire national de métrologie et d’essais, Paris, FRANCE, March 26, 2013.
- [23] D. E. Fagnan, J. Wang, C. Zhu, P. Djuricanin, B. G. Klappauf, J. L. Booth, and K. W. Madison, *Phys. Rev. A* **80**, 022712 (2009).
- [24] J. Van Dongen, C. Zhu, D. Clement, G. Dufour, J. L. Booth, and K. W. Madison, *Phys. Rev. A* **84**, 022708 (2011).
- [25] J. Scherschligt, J. A. Fedchak, D. S. Barker, S. Eckel, N. Klimov, C. Makrides, and E. Tiesinga, *Metrologia* **54**, S125 (2017).
- [26] J. Scherschligt, J. A. Fedchak, Z. Ahmed, D. S. Barker, K. Douglass, S. Eckel, E. Hanson, J. Hendricks, N. Klimov, T. Purdy, J. Ricker, R. Singh, and J. Stone, *Journal of Vacuum Science & Technology A* **36**, 040801 (2018).
- [27] S. Eckel, D. S. Barker, J. A. Fedchak, N. N. Klimov, E. Norrgard, J. Scherschligt, C. Makrides, and E. Tiesinga, *Metrologia* **55**, S182 (2018).
- [28] P. Shen, K. W. Madison, and J. L. Booth, *Metrologia* **57**, 025015 (2020).
- [29] P. Shen, K. W. Madison, and J. L. Booth, *Metrologia* **58**, 022101 (2021).
- [30] R. A. Stewart, P. Shen, J. L. Booth, and K. W. Madison, *Phys. Rev. A* **106**, 052812 (2022).
- [31] L. H. Ehinger, B. P. Acharya, D. S. Barker, J. A. Fedchak, J. Scherschligt, E. Tiesinga, and S. Eckel, *AVS Quantum Science* **4**, 034403 (2022).
- [32] P. Shen, E. Frieling, K. R. Herperger, D. Uhlund, R. A. Stewart, A. Deshmukh, R. V. Krems, J. L. Booth, and K. W. Madison, *New Journal of Physics* **25**, 053018 (2023).
- [33] D. S. Barker, J. A. Fedchak, J. Kłos, J. Scherschligt, A. A. Sheikh, E. Tiesinga, and S. P. Eckel, *AVS Quantum Science* **5**, 035001 (2023), <https://pubs.aip.org/avs/aqs/article-pdf/doi/10.1116/5.0147686/18068991/035001.1.5.0147686.pdf>.
- [34] V. B. Makhalov, K. A. Martinyanov, and A. V. Turlapov, *Metrologia* **53**, 1287 (2016).
- [35] V. B. Makhalov and A. V. Turlapov, *Quantum Electronics* **47**, 431 (2017).
- [36] A. Deshmukh, “A model of quantum diffractive heating,” personal communication (2023), talk at the Quantum Sensors for Vacuum Metrology, Vancouver, Canada, May 12, 2023.
- [37] S. e. a. Eckel, “in preparation,” (2023).
- [38] A. A. Medvedev, V. V. Meshkov, A. V. Stolyarov, and M. C. Heaven, *Phys. Chem. Chem. Phys.* **20**, 25974 (2018).
- [39] J. R. Gardner, G. Pleiss, D. Bindel, K. Q. Weinberger, and A. G. Wilson, in *Advances in Neural Information Processing Systems* (2018).